RESPONSE TO REVIEWER 1: First Report on Coseismic Ionospheric Disturbances Following the Deep-Focus Earthquake (Mw 6.6) in Tarauacá, Acre, Brazil: Ground Uplift and TEC Analysis

Adebayo et al. (2024)

December 2024

We appreciate the reviewer for this invaluable comments and suggestions. The contributions have helped us to improve the quality of the manuscript. We modified the manuscript based on the reviewer's comments and suggestions.

Comment on the manuscript entitled "First Report on Coseismic Ionospheric Disturbances Following the Deep-Focus Earthquake (Mw 6.6) in Tarauacá, Acre, Brazil: Ground Uplift and TEC Analysis" by Adebayo et al.

This manuscript investigates ionospheric disturbances associated with a magnitude 6.6 deep-focus earthquake in Tarauacá, Brazil, occurred on January 20, 2024. Despite the epicenter being located at a depth of 607 km, and no significant surface damage reported, TEC variations related to this earthquake were detected. One of the most noteworthy aspects of this study is the observation of ionospheric disturbances following such a deep-focus earthquake. However, there are several methodological issues and uncertainties in the analysis and interpretation of the data that require clarification.

- The authors assert that Figure 2 illustrates N-shaped disturbances, commonly reported as coseismic ionospheric disturbances in TEC data. While the TEC disturbance in amcoG17 may exhibit N-type characteristics, the variation in amteG09 may not be recognized as this pattern.

  To ensure that the large intensification of ΔTEC in Figure 2 are coseismic ionospheric disturbances, the travel-time diagram in Figure 3 is presented. The diagram connects the N-shaped disturbances at amcoG17 to the large intensification at amteG09. Moreover, before concluding that the TEC signatures are associated with the earthquake, we carefully considered several criteria that the observed disturbances must satisfy: **Ionospheric Quietness:** For TEC disturbances from a deep-focus earthquake to be clearly visible, the ionosphere must be in a quiet state. To confirm this, we obtained the DST profile for the day of the event and for the entire

month of January 2024. As shown in Figure S2, the ionosphere was exceptionally quiet on the day of the event and throughout January 2024, particularly in the equatorial region. **Spatial Consistency:** If the TEC disturbance were merely coincidental or a random ionospheric fluctuation, it would likely be observed in a single receiver or along a single trajectory. However, we observed the "N-shaped" disturbance along two satellites and four receivers, located at different positions around the earthquake epicenter, demonstrating a clear, spatially consistent pattern. **Radial Propagation:** Finally, if the TEC disturbance were linked to the earthquake, we would expect certain features, such as the radial propagation of disturbances away from the epicenter. This was clearly observed in the travel-time diagram of the disturbance, supporting its seismic origin. In summary, the TEC disturbances observed in our data satisfy all three of these criteria, strongly supporting their association with the earthquake.

- Furthermore, the authors state that the onset of the amteG09 disturbance occurred 330 seconds after the earthquake. Assuming the TEC disturbance occurred at an altitude of 250 km, the propagation speed of acoustic waves is faster than normal speed, as shown in Figure S1. If the wave propagation speed was typical, the disturbance would need to have occurred at a lower altitude. The authors must clarify the altitude at which the TEC disturbances were detected.

Recent reports on rapid detection, earlier than 480 seconds, are explained, based on AGWs simulation (Sanchez et al, 2024). The study by Sanchez et al (2024) overcomes the limitation of ray tracing and explains the detection of CSID as early as 350 seconds at 250 km altitude. Sanchez et al (2024) explained such early detection as follows: "From the ground uplift, numerous waves with wavefronts of different slops that is, of different phase speeds are launched into the atmosphere. This is owing to the numerous scale heights and duct sizes present in the atmosphere, that allow numerous wavelengths at a given frequency to be sustained in the atmosphere. The waves with significant amplitudes arrive at 160 km the waves arrive in about 240 s from the onset. These waves have wavelengths comparable to the size of the longest atmospheric duct of about 150 km and at the acoustic frequencies, they propagate with a phase speed of about 600 m/s or more. Therefore, in the rapid development of ionoquakes, the long wavelength AGWs participate, as also found by Kherani et al. (2012)." We have included more discussion on Figure 3 in line 205-216 in the manuscript.

Lowering the altitude to explain the early detection is inconsistent since it is based on the ray-tracing technique. For example, for the Sanriku-Oki earthquake, Thomas et al (2018) reported the early detection in 420 seconds using ray tracing technique and explained it by lowering the altitude to 130 km. However, for the same event, the study by Astafyeva et al (2013) reports the detection altitude of a majority of CSIDs at 200-250 km altitude. The work by Sanchez et al (2023) confirms the finding

of Astafyeva et al (2013) and explains the early detection based on the mechanism described above.

- One of the reasons for these discrepancies may be the determination of the TEC variation onset time. As suggested in Bagiya et al. (2023), the influence of multiple sources of ground motion could explain deviations in the N-shaped TEC disturbance patterns. The disturbances associated with the earthquake need to be precisely identified and their characteristics analyzed in detail.

  The detection time method the present study is based on the time of peak value of intensified ΔTEC oscillation immediately after the EQ onset, proposed by Maletckii and Astafyeva, (2021) and Sanchez et al (2023). Such estimation is unambiguous since the peak can be identified unambiguously. For this reason, we estimate the detection time, based on the peak of ΔTEC. The detection time estimation based on the beginning time of ΔTEC is not certain owing to the contribution from non-seismic sources and we avoid such a method in the present study..

- The methods employed for TEC data analysis, as presented in Figures 4–6, raise further concerns. The authors compared the normalized average of dTEC data with 15-second sampled ground motion data, concluding that N-type variations correlate with ground motion. However, it is unclear which specific ground motion peaks correspond to the TEC variations. Figure 4 is complemented by Figure 5 to show that the large uplift causes large ΔTEC till a certain frequency. Therefore the peak ΔTEC, which is used in the detection time estimation, is caused by maximum uplift at that frequency. However, whole N-shaped ΔTEC has contribution from lower acoustic frequencies each of which shows a distinct peak in ground uplift. We have included more discussion for the Figure 4 (see line 243-261).

- Using this normalized average of dTEC data, the authors also performed a frequency analysis on the TEC disturbances as shown in Figure 5. Then Figure 6 shows the relationship between ground motion and TEC disturbances. However, it is necessary to take into account the distance between the epicenter location and the IPP and evaluate the attenuation of the acoustic wave during the propagation from the ground to the IPP to compare the ground motion and the ionospheric disturbances quantitatively. Given that the trajectories of the four IPPs vary in distance from the epicenter, the TEC data should be corrected for these distances before making quantitative comparisons with ground motion. The normalization of dTEC data neglects these attenuation effects, leading to potential inaccuracies in comparing the intensities of ground motion and the TEC variations.

  To understand the effects of IPP location on spectral behavior in Figures 5-6, we present below spectral results for each receiver-satellite geometry (Figure S3). We note that the behavior remains the same qualitatively.

The normalization is not an issue since the spectral behavior remains similar for each receiver-satellite geometry. On the other hand, to have the quantitative assessment, we present figures 6 without normalization (Figure S4) and it can be seen that the results remain the same. The figures below are also without normalization. The spectral behavior of Figures 5-6 are inline with the theoretical understanding. Therefore, normalization or no-normalization, it does not alter the physics.

Reviewer Recommendation: Based on the outlined concerns, the reviewer thinks that this manuscript includes serious problems in the interpretation of the observation results and the method of the data analysis. Therefore, the reviewer thinks that this paper should be rejected for publication in Angeo.

Specific Comments:

L86: Replace "slight" with "slant."

We have replaced the "slight" with "slant"

L96: Clarify whether "sTEC" refers to the same data as "TEC" mentioned in L99.

Yes.

Figure 1: Indicate which satellite-receiver combinations correspond to the four IPP trajectories.

We have indicated the satellite-receiver combinations that correspond to the four IPP trajectories in Figure 1.

L157 "dTEC obtained from the sTEC data is shown in (b1) and (b2). These two receivers observe a clear N-type wave pattern ... " : The TEC variation in (b1) may appear N-type; however, (b2) is unlikely to exhibit an N-type pattern. Additionally, the onset time of (b2) disturbances must be explicitly stated, as this is critical for evaluating propagation delays.

This has been answered in the second bullet-point above.

L161"The figure illustrates that ground uplift took off at 21:55 UT": The ground uplift timing inferred from the figure appears to be 21:33, not 21:55 as mentioned.

The time in the Figure 2 are in hours converted as thus: (time (UT) = t_{obs} hr + (minutes/60) hr + (seconds/3600) hr). We have included this information in Figure 2 caption.

L162 "This delay could be attributed to the distance between the seismometer and the earthquake epicenter which is 788 km.": Sometimes a technical term "epicenter" uses the following two meanings. One is the position of the hypocenter on the earth's surface. The other is the hypocenter itself. Which did the authors used for this term?

According to USGS, "The location below the earth's surface where the earthquake starts is called the hypocenter, and the location directly above it on the surface of the earth is called the epicenter." (`https://www.usgs.gov/programs/earthquake-hazards/science-earthquakes`). Thus, the epicenter term in the manuscript means the location directly above the point where the earthquake starts.

Figure 2: Verify if the ground motion data were corrected for the seismometer's frequency response. Broadband seismometers often lack sensitivity below 10 mHz (Nakata et al., 2021). When quantitatively comparing ground motions and TEC variations, such as those shown in Figure 6, the sensitivity of the seismometer should be corrected.

Yes, we corrected the seismometer's frequency response by using the ObsPy Python Library. We included the following in the manuscript (under the Data and Methods) for better clarification: "ObsPy is an open-source tool designed for querying, retrieving, processing, and managing seismological datasets (Hosseini and Sigloch, 2017). The library facilitates downloading data in count format, estimating ground vibrations, and minimizing the effects of instrumental responses, including those from the frequency response, amplifier, analog and digital filters, and digitization."

L194 "In addition, "AMTE" detected ionoquakes earlier, starting at 330 seconds (5.5 minutes),": If the "amte-G09" disturbance onset is 330 seconds after the earthquake, its propagation to the IPP at 250 km altitude seems improbable. Clarify whether the disturbance occurred at a lower altitude and specify the altitude in question.

This has been answered in the second bullet-point above.

L206: Detail how the profile of the acoustic wave shown in Figure S1 was determined.

We used the atmospheric data from MSIS model to calculate the sound speed profile. We have also included this information in the Figure S1.

Figure 3: The latitude-based ordering of IPP trajectories does not align with distances from the epicenter. For instance, the easternmost IPP (AMTE?) is closer to the southernmost IPP (CRUZ?) in terms of distance from the epicenter. In the figure, the acoustic wave propagation is indicated by arrows, but it is doubtful whether these arrows represent the correct propagations of the acoustic waves.

The arrows in Figure 3 show the clear acoustic wave propagation as detected along the trajectories of PRN 09 and PRN 17 observed by the receivers. However, it seems the confusion is due to the absence of the satellite-receiver combinations which we have now included in the Figure 1. We believe that should resolve the issue.
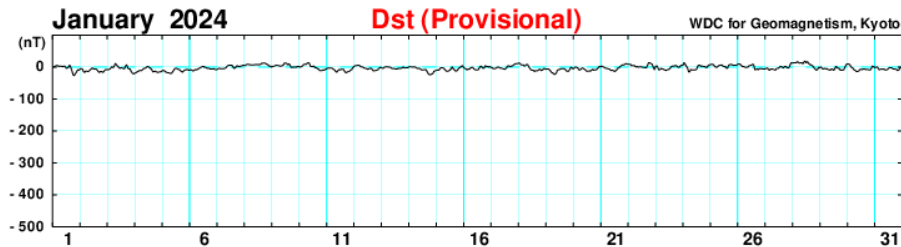
Figure S2: Dst for the month of January 2024 obtained from `https://wdc.`
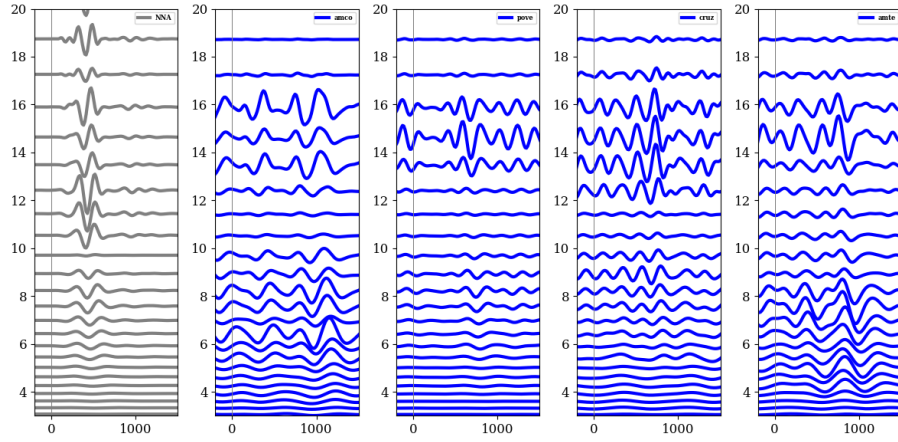
Figure S3: Spectrogram of each of the receiver and the ground uplift. The frequency distribution is similar.
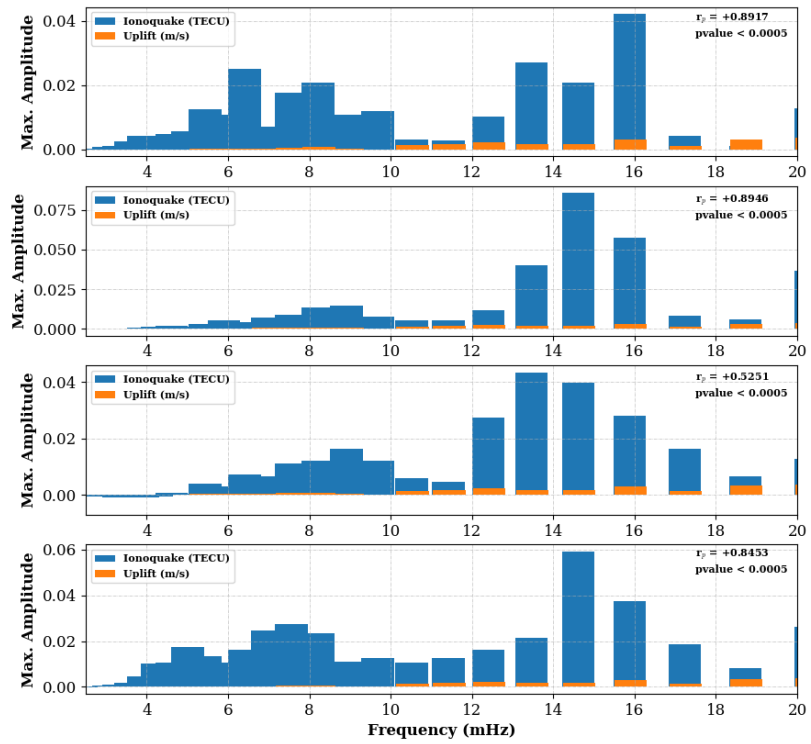
Figure S4: Ground uplift and the TEC maximum amplitude for each receiver.
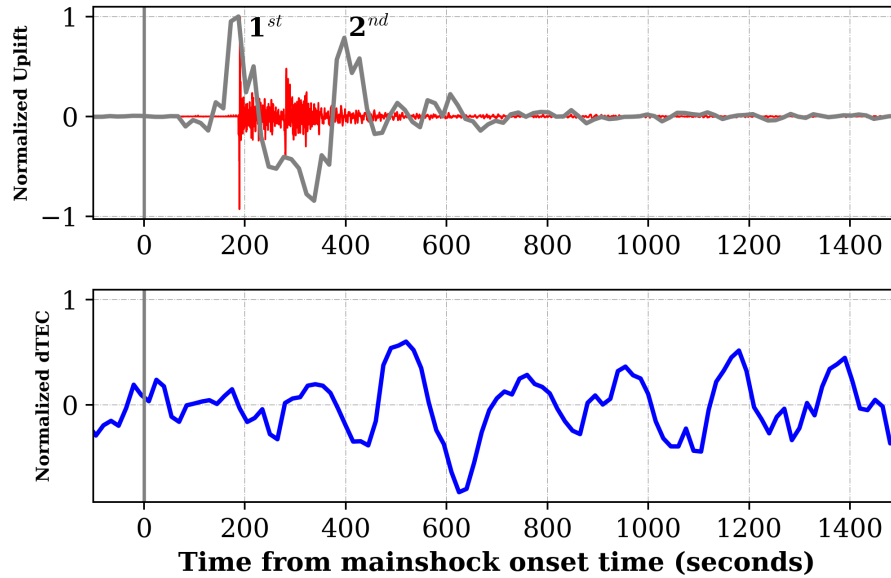
Figure 4: Upper panel shows the resampled (15 seconds) normalized ground uplift (in grey), the original uplift data (in red) and lower panel is the normalized average of the dTEC from the receivers in figure 3.

References:

Bagiya, M. S., Heki, K., Gahalaut, V. K. (2023). Anisotropy of the near-field coseismic ionospheric perturbation amplitudes reflecting the source process: The 2023 February Turkey earthquakes. Geophysical Research Letters, 50, e2023GL103931.

Nakata, H., Takaboshi, K., Takano, T., Tomizawa, I. (2021). Vertical propagation of coseismic ionospheric disturbances associated with the foreshock of the Tohoku earthquake observed using HF Doppler sounding. Journal of Geophysical Research: Space Physics, 126, e2020JA028600. `https://doi.org/10.1029/2020JA028600` Sanchez, S. A., Kherani, E. A. (2024). A New Analytical Simulation Code of Acoustic-Gravity Waves of Seismic Origin and Rapid Co-Seismic Thermospheric Disturbance Energetics. Atmosphere, 15(5), 592. `https://doi.org/10.3390/atmos15050592` Maletckii, B., Astafyeva, E. (2021). Determining spatio-temporal characteristics of coseismic travelling ionospheric disturbances (CTID) in near real-time. Scientific Reports, 11(1), 20783. Sanchez, S. A., Kherani, E. A., Astafyeva, E., De Paula, E. R. (2023). Rapid Detection of Co-Seismic Ionospheric Disturbances Associated With the 2015 Illapel, the 2014 Iquique and the 2011 Sanriku-Oki Earthquakes. Journal of Geophysical Research: Space Physics, 128(9), e2022JA031231. Thomas, D., Bagiya, M. S., Sunil, P. S., Rolland, L., Sunil, A. S., Mikesell, T. D., ... Ramesh, D. S. (2018). Revelation of early detection of co-seismic ionospheric perturbations in GPS-TEC from realistic modelling approach: Case study. Scientific reports,

8(1), 12105. Astafyeva, E., Shalimov, S., Olshanskaya, E., Lognonné, P. (2013). Ionospheric response to earthquakes of different magnitudes: Larger quakes perturb the ionosphere stronger and longer. Geophysical Research Letters, 40(9), 1675-1681. Sanchez, S. A., Kherani, E. A. (2024). A New Analytical Simulation Code of Acoustic-Gravity Waves of Seismic Origin and Rapid Co-Seismic Thermospheric Disturbance Energetics. Atmosphere, 15(5), 592.